Received: 1 February 2022 | Revised: 8 May 2022 | Accepted: 31 May 2022

DOI: 10.1002/mrm.29367

RESEARCH ARTICLE

Magnetic Resonance in Medicine

Macromolecular background signal and non-Gaussian metabolite diffusion determined in human brain using ultra-high diffusion weighting

Kadir Şimşek[1,2,3] | **André Döring**[4] | **André Pampel**[5] | **Harald E. Möller**[5] | **Roland Kreis**[1,3]

[1]Magnetic Resonance Methodology, Institute of Diagnostic and Interventional Neuroradiology, University of Bern, Bern, Switzerland

[2]Graduate School for Cellular and Biomedical Sciences, University of Bern, Switzerland

[3]Translational Imaging Center (TIC), Swiss Institute for Translational and Entrepreneurial Medicine, Bern, Switzerland

[4]Cardiff University Brain Research Imaging Centre (CUBRIC), School of Psychology, Cardiff University, Cardiff, UK

[5]Max Planck Institute for Human Cognitive and Brain Sciences, Leipzig, Germany

Correspondence
Prof. Dr. sc. nat. Roland Kreis, MR Methodology, University Bern, Freiburgstr. 3, CH-3010 Bern, Switzerland.
Email: roland.kreis@insel.ch

Funding information
Swiss National Science Foundation, Grant/Award Numbers: 202962, 320030-175984

Purpose: Definition of a macromolecular MR spectrum based on diffusion properties rather than relaxation time differences and characterization of non-Gaussian diffusion of brain metabolites with strongly diffusion-weighted MR spectroscopy.

Methods: Short echo time MRS with strong diffusion-weighting with *b*-values up to 25 ms/μm^2 at two diffusion times was implemented on a Connectom system and applied in combination with simultaneous spectral and diffusion decay modeling. Motion-compensation was performed with a combined method based on the simultaneously acquired water and a macromolecular signal.

Results: The motion compensation scheme prevented spurious signal decay reflected in very small apparent diffusion constants for macromolecular signal. Macromolecular background signal patterns were determined using multiple fit strategies. Signal decay corresponding to non-Gaussian metabolite diffusion was represented by biexponential fit models yielding parameter estimates for human gray matter that are in line with published rodent data. The optimal fit strategies used constraints for the signal decay of metabolites with limited signal contributions to the overall spectrum.

Conclusion: The determined macromolecular spectrum based on diffusion properties deviates from the conventional one derived from longitudinal relaxation time differences calling for further investigation before use as experimental basis spectrum when fitting clinical MR spectra. The biexponential characterization of metabolite signal decay is the basis for investigations into pathologic alterations of microstructure.

KEYWORDS

apparent diffusion constants, diffusion, brain, fitting, macromolecules, microstructure, modeling, MR spectroscopy, quantification

1 | INTRODUCTION

Proton MR spectroscopy (^{1}H-MRS) offers noninvasive insights into brain metabolism and provides a tool for noninvasive diagnosis and monitoring. ^{1}H-MR spectra obtained at short TEs provide best SNR for quantification of brain metabolites. However, signals from macromolecules (MMs)[2–4] that overlap with the small molecular metabolite signals and are not predefined by knowledge about their composition and concentrations complicate quantification at short TE.[4–6] For most accurate and robust quantification of metabolite tissue contents, it is, thus, recommended to use an experimental MM spectrum as part of the basis set for linear combination model fitting. Furthermore, absolute quantification of MM signals in terms of tissue content and variation in composition may inherently carry information on pathologies.[4,7] MM resonance characteristics are distinct from those of small metabolites by considerably shorter T_1 and T_2 relaxation times[2,3,8,9] and up to 20 times smaller apparent diffusion coefficients (ADCs).[10] This has been exploited to define a macromolecular background (MMBG) spectrum to be used in quantification or as entity of clinical interest. The short T_2 is the basis for using mathematical models to define or compensate for MMBG signals.[5,11–13] Relying on T_1 differences, single[3] or double[14] inversion recovery techniques have been used to null metabolite signals and to determine an experimental MMBG pattern for specific acquisition settings. Similarly, a combination of saturation or inversion recovery scans with specific postprocessing[15] or multidimensional modeling[16,17] have been applied for the same aim. Finally, the differences in ADC values in combination with metabolite-nulling have been the basis for combined T_1 and diffusion-weighting based definition of the MMBG in rodents on a preclinical scanner[18] with much higher gradient strength than available on standard clinical scanners.

In addition to serving as a tool to differentiate metabolites from MMs, diffusion-weighted MRS (DW-MRS) has also become a contender for the elucidation of brain microstructure.[19–21] The main gain when switching from water to metabolites as diffusion probes is the fact that unlike water, most metabolites reside almost exclusively in intracellular space, and some of them have even a celltype-specific origin. *N*-acetylaspartate (NAA) and glutamate (Glu) are known as neuronal markers, while myo-inositol (mI), glutamine (Gln) and, possibly to a lesser extent, total choline compounds (tCho) are assumed to be glial markers.[21] Therefore, the diffusion characteristics of these metabolites provide specific microstructural information without having to rely on modeling of exchange and assumptions on compartment properties as for water. One challenge originates from the fact that metabolite diffusion coefficients are considerably smaller than those of water, which implicates that higher diffusion weighting has to be applied for substantial DW contrast. Unfortunately, on clinical MR scanners, strong diffusion-weighting implicates the use of longer TE, which makes observation of non-singlet metabolites difficult, and/or STEAM with inherently lower SNR—in particular if non-Gaussian diffusion or the determination of the MMBG pattern is targeted, both depending on heavy signal diminution of metabolite signals.

The current study aimed at establishing DW-MRS on a Connectom scanner with very large gradient strength[22] for investigating human subjects at comparable TE as used in clinical spectroscopy. A DW-weighted STEAM sequence[23] with highest diffusion-weighting allowed by peripheral nerve stimulation and offering simultaneous acquisition of metabolite and water signals was used in combination with multidimensional simultaneous fitting of spectral and diffusion decay information to define a MMBG spectral pattern devoid of residual metabolite signals that can be compared with T_1-based MMBG patterns. In addition, the study aimed at determination of non-Gaussian diffusion characteristics for a wide range of metabolites, including those that are primarily observable at short TE.

2 | METHODS

The details of methods are given in the Supporting Information Text S1 in Appendix S1, which is available online, while the following description is limited to the basic principles.

2.1 | Experimental setup and data acquisition

Most measurements were performed on a 3T-MAGNETOM Skyra Connectom-A (Siemens Healthineers) with 300 mT/m per gradient axis.

Localization was carried out by STEAM[23] applying trapezoidal diffusion gradients. The sequence is determined by TE, the mixing time TM, the duration of diffusion gradients δ, and the nominal diffusion time Δ. The calculated diffusion-weighting term *b* includes contributions from all gradients and cross-terms.

Metabolite-cycling served as water-elimination method providing simultaneous records of water diffusion and reference signals for motion compensation.[23]

Phantom measurements were carried out to determine the maximum diffusion-weighting within the peripheral nerve and cardiac stimulation (PNS/CS) limits.[24] A PNS/CS simulation tool[25,26] was used as a guide in devising

the experimental parameters aiming for short TE and moderate TM. Two protocols with TM/Δ values of 35/50 ms and 65/80 ms were defined for TE = 30 ms, both aimed at MMBG determination (maximal *b*-value at minimal TE/TM for consistency with clinical MRS) rather than evaluation of diffusion-time dependence of ADCs. For Δ = 50 ms, six *b*-values from 0.38 to 10.71 ms/μm^2 and for Δ = 80 ms, 11 *b*-values from 0.37 to 25.1 ms/μm^2 were recorded. The highest generally feasible gradient strength was 140 mT/m per axis.

Twelve healthy subjects (7 female, age 28 ± 5.2 years) were examined with a volume of interest (VOI) of 23 ± 4 cm^3 in occipito-parietal cortex. Acquisition parameters included: 64 acquisitions, 4000 Hz spectral width, TR dictated by peripheral-pulse triggering with a minimum of 1.8 s. The effective TR (TR^{eff}) was tracked using time stamps. Scans with metabolite-nulling and the same sequence were recorded in separate sessions and subjects.

All scans were performed in accordance with the competent ethical review boards.

2.2 | Processing

Processing was performed in MATLAB (incl. Data preparation[27,28]), Python, jMRUI[29] and FiTAID.[16,30] jMRUI[29] was used for creation of cohort-average spectra following application of two motion-compensation schemes. Nineteen spectra with artifacts were excluded from cohort-averaging.

2.2.1 | Motion compensation

The previously described water-signal based motion-compensation[23] (W-MoCom) includes amplitude restoration. Since the water signal amplitudes are influenced by irregular heart rates, a correction factor $(1-\exp[-TR^{eff}/T_1])$ was applied to each acquisition before definition of reference level (top quartile of scans) for subsequent amplitude-upscaling. Figure 1 illustrates the effect on water reference levels for illustrative DW measurements. Typically, the TR-correction increased the reference level. The effect was strongest when heart-rate fluctuations caused TR^{eff} to jump from two to three or even four RR periods.

The second stage of compensation for motion-related signal loss (M-MoCom) was based on the MM resonance at ~0.9 ppm.[31]1 At first, internal gold-standard diffusion decay for this signal area was formed from individual datasets of best quality. This was subsequently used to upscale individual *b*-value spectra for all subjects such that

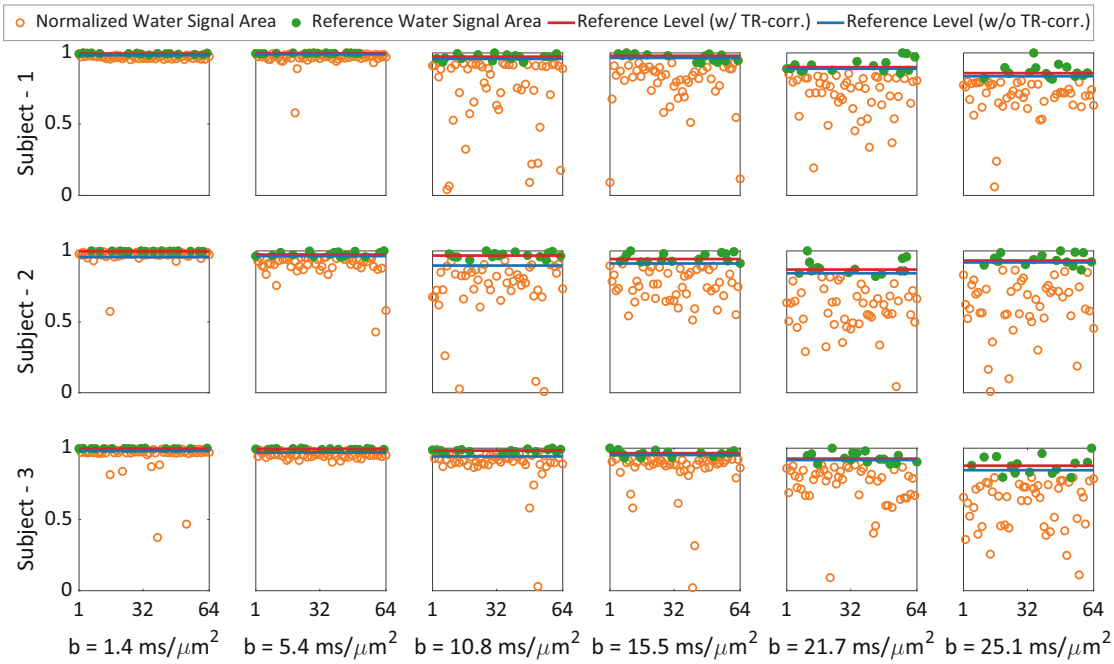

FIGURE 1 Illustration of the definition of the reference level for the water signal used for the W-MoCom correction scheme and the effect of TR^{eff} correction. Normalized signal intensities (orange) of single acquisitions from three subjects are plotted in order of their recordings (areas of a Voigt line fitted to the water peak). Areas are shown after TR^{eff} correction for variance in T_1 saturation due to physiologic changes in heart rate. The reference level was defined as the median of the top quartile of all acquisitions (green). The W-MoCom reference levels are illustrated before (blue line) and after (red line) TR correction. (For ease of illustration, water signal intensities were normalized with the highest intensity obtained from each scan.)

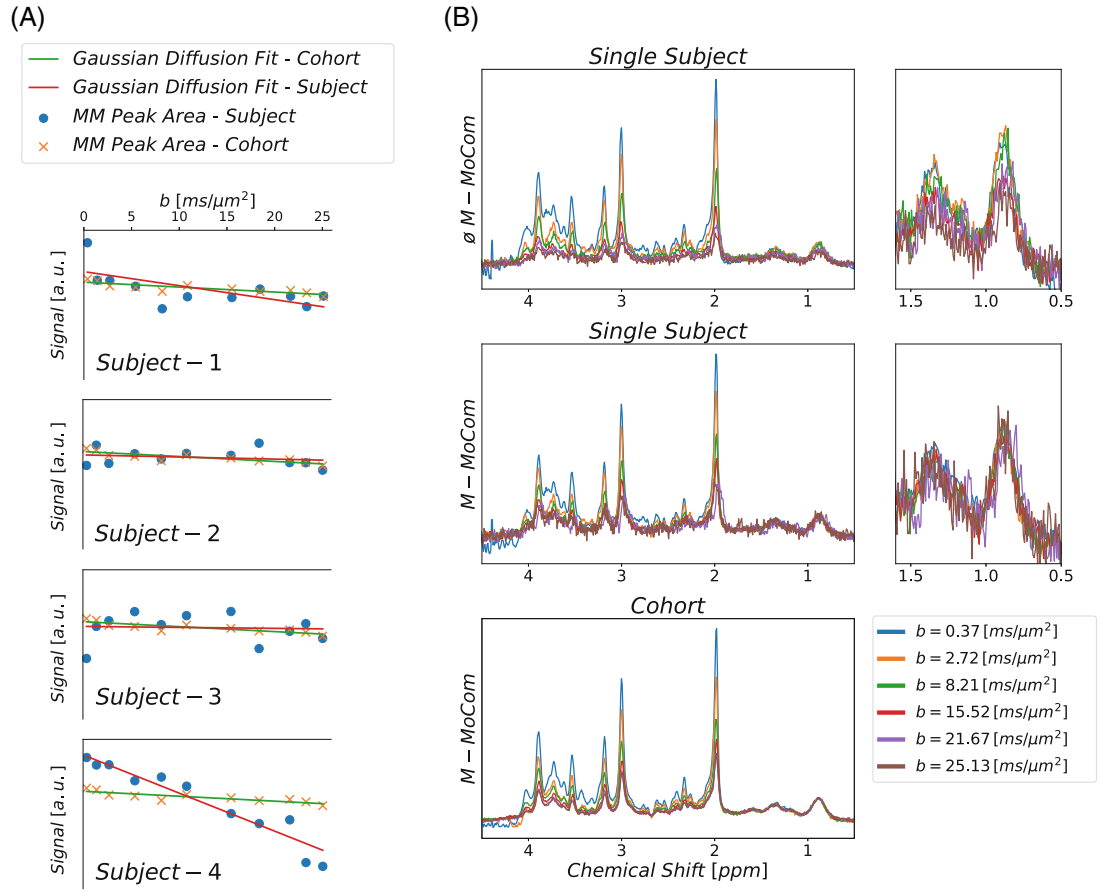

FIGURE 2 Illustration of the motion correction scheme M-MoCom for multiple subjects. A, The individual $M_{0.94}$ areas estimated for each *b*-value are plotted in comparison to the monoexponential fit for the specific subject and the whole cohort. Orange crosses represent the averaged $M_{0.94}$ areas over all subjects, whereas the blue dots correspond to $M_{0.94}$ areas obtained from a single subject. The green line indicates the reference diffusion decay obtained from a monoexponential fit of cohort-averaged areas (from six subjects). Subject 4 shows a systematically motion-corrupted signal decrease, whereas subjects 2 and 3 feature single spectra with apparent signal drops. B, Spectra obtained from a single subject (subject 4) are depicted for six *b* values before (top) and after (middle) M-MoCom. The effect of M-MoCom is best appreciated in the zoomed panels. The cohort spectra after M-MoCom are presented at the bottom.

they all showed the same monoexponential decay for this MM peak. The resulting monoexponential fit provided the undistorted diffusion decay for the whole MMBG pattern with an $ADC_{M0.94}$ of $(3.4 \pm 0.7) \times 10^{-3}$ μm²/ms ($R^2 = 0.74$). Figure 2A illustrates individual diffusion attenuations of $M_{0.94}$ in comparison to the reference decay from the cohort-average from six subjects. The deviations of the $M_{0.94}$ peak signal are the base for the correction factors for M-MoCom.

2.2.2 | Data fitting

Spectra were fitted in FiTAID[30] in a 2D-fashion as connected series of spectra including all different DW spectra. The model included 19 metabolites and a MMBG signal representation consisting of equally spaced Voigt lines with identical Gaussian and Lorentzian broadening. Prior knowledge between the *b*-value spectra could include monoexponential or biexponential signal decay. Where no diffusion signal behavior was enforced in FiTAID, the signal decay was subsequently fitted in Python.

Table 1 charts all simultaneous and sequential fit strategies used for the analysis of metabolite diffusion and creation of MMBG patterns. The metabolites were divided into two categories, named *major* and *minor metabolites*, where a biexponential signal decay representation was only fitted with full flexibility for major metabolites. The major metabolites were Glu, Gln (some models only), mI, NAA, tCho, and total creatine (tCr; Cr + PCr). This choice was based on expected size of signal contribution, initial fit results, and non-Gaussian diffusion characteristics in mouse brain.[32,33]

In Table 1, "simultaneous spectral/diffusion modeling" specifies whether diffusion signal decay was enforced in FiTAID, reducing the area-related fit parameters to 2

TABLE 1 Overview of all fit strategies used in this study: Two main fitting procedures govern the various strategies

Case label	*b*-Values used [ms/μm²]	MMBG pattern estimation	Simultaneous spectral fit/ diffusion modeling		Case label	*b*-Values used [ms/μm²]	Subsequent diffusion modeling	
			Major metabolites	Minor metabolites			Major metabolites	Minor metabolites
SF-A	all	monoexp	✘	✘	**SF-A1**	<11	monoexp	monoexp
					SF-A2	all	biexp	monoexp
					SF-A3	all	biexp	$biexp_{con}$
SF-B	all	monoexp	✘	monoexp	**SF-B1**	<11	monoexp	✘
					SF-B2	all	biexp	✘
SF-C	<11	monoexp	monoexp	monoexp	✘	✘	✘	✘
SF-D	all	monoexp	biexp	monoexp	✘	✘	✘	✘
SF-E	all	monoexp	biexp	$biexp_{con}$	✘	✘	✘	✘
SF-F	<6	✘	monoexp	monoexp	✘	✘	✘	✘

Note: The simultaneous spectral fit / diffusion modeling represents the simultaneous two-dimensional signal modeling in FiTAID, whereas the subsequent diffusion modeling comprises the diffusion signal decay analysis in Python using estimated metabolite areas found for a spectral fit without diffusion constraints in spectral fitting.
Abbreviations: biexp, biexponential signal representation; $biexp_{con}$, constrained biexponential signal representation; monoexp, monoexponential signal representation.

for monoexponential (Equation 1) and 4 for biexponential decay (Equation 2). If no amplitude relation was enforced in FiTAID independent area fit variables per *b*-value were estimated in FiTAID and the "subsequent diffusion modeling" was performed in Python.

$$S(b) = S_0 e^{(-b\mathrm{ADC})} \tag{1}$$

$$S(b) = S_0 \left(f_{\mathrm{fast}} e^{(-b\mathrm{ADC}_{\mathrm{fast}})} + (1 - f_{\mathrm{fast}})\, e^{(-b\mathrm{ADC}_{\mathrm{slow}})} \right) \tag{2}$$

For pure monoexponential analyses, limited *b*-value ranges were chosen. For biexponential fitting, boundaries for metabolite ADCs were based on mouse data[32]: 0.10–0.25 μm²/ms for the fast and 0.01–0.10 μm²/ms for the slow component. For water, the division was at 0.3 μm²/ms. The whole MMBG signal was always modeled with monoexponential decay and predefined ADC (see M-MoCom procedure).

SF-A3, SF-E, and SF-F were developed based on results from other fit strategies and to best represent diffusion decays respecting underlying signal decay representations, appropriate *b*-value ranges, while limiting the number of free fit variables. For SF-E, aimed at the conclusive definition of the diffusion-based MMBG and best estimation of biexponential decays, minor metabolites were represented by a constrained biexponential model where only ADC_{fast} and the total signal were estimated while f_{fast} was fixed at 0.5 and ADC_{slow} at 0.03 μm²/ms (based on Refs[10,32] and our initial results for major metabolites). SF-F was devised to obtain most robust monoexponential ADCs to be compared to literature (using *b*-values <6 ms/μm²). Individual subject data were fitted for SF-A, SF-C, and SF-D.

3 | RESULTS

Figure 3 presents postprocessed spectra for a single subject and the cohort average for both diffusion times. The spectral quality of both datasets is excellent in terms of SNR and linewidth. The metabolite contributions show the expected strong diffusion decay, while the MMBG signals remain little affected throughout. The main focus is placed on the data with longer diffusion time and higher *b*-values while the results for shorter TM are mostly provided in the Supporting Information.

Figure 4 illustrates the fit results for all spectral fitting models for the lowest, an intermediate, and the highest diffusion-weighting. The residues are largest for the lowest *b*-value throughout and the shape and magnitude of the residuals is similar between fit strategies. The fit results for Δ = 50 ms are provided in Figure S2 in Appendix S1.

3.1 | Diffusion properties of metabolites

The ADC results of monoexponential diffusion analysis at Δ = 80 ms for the most intense metabolites are listed in Table 2. Corresponding diffusion decays are illustrated in Figure 5A. Corresponding data for Δ = 50 ms can be found in Supporting Information Table S3 and Figure S4 in Appendix S1. Estimated monoexponential ADCs for

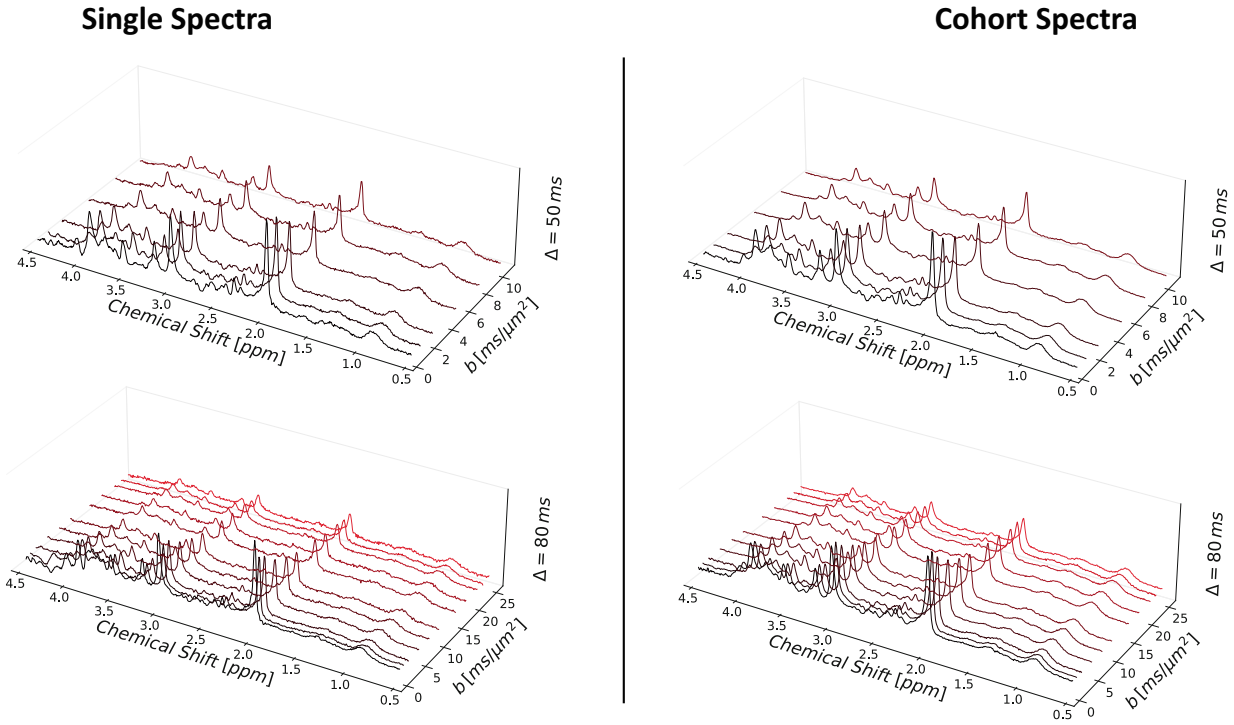

FIGURE 3 Spectra obtained from a single subject (left) and cohort average spectra (right) are illustrated for both diffusion times. The upper part contains the spectra for TM/Δ = 35/50 ms with six *b* values up to 10.7 ms/μm². The spectra at the bottom were recorded with TM/Δ = 65/80 ms and with 11 different *b* values up to 25.1 ms/μm².

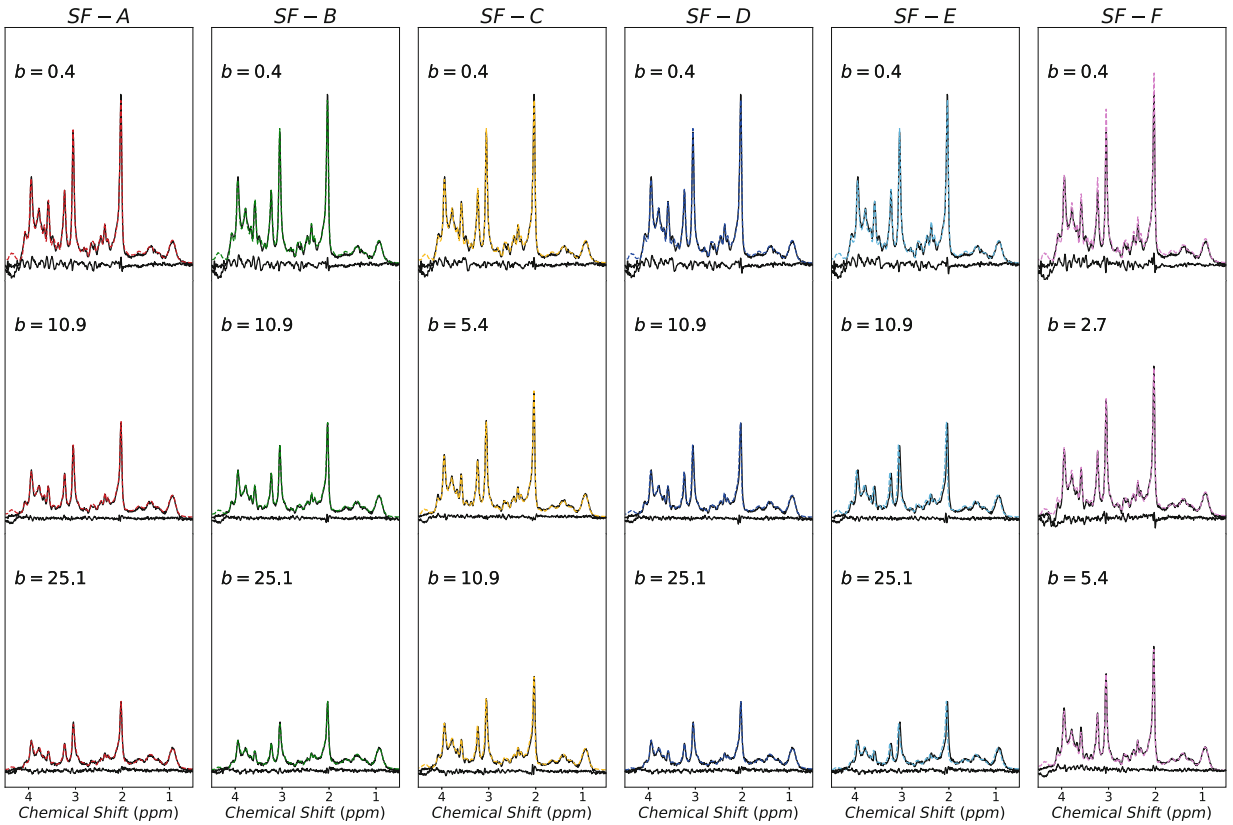

FIGURE 4 Sample spectral fit results from all fitting procedures at Δ = 80 ms. Experimental (black), fitted (color-coded), and residual signal (black) spectra are illustrated for three selected *b* values in the cohort average spectrum. (b values in units of ms/μm².)

TABLE 2 Estimated ADCs of metabolites for monoexponential signal decay at $\Delta = 80$ ms from fitting the cohort average spectra in a restricted *b*-value range

	Monoexponential diffusion fit			
	ADC [$\mu m^2/ms$]			
Metabolites	**SF-A1**	**SF-B1**	**SF-C**	**SF-F**
Aspartate	0.133 ± 0.044	0.172 ± 0.009[a]	0.250 ± 0.025[a]	0.046 ± 0.006[a]
Glutamate	0.079 ± 0.008	0.079 ± 0.006	0.106 ± 0.003[a]	0.115 ± 0.002[a]
Glutamine	0.123 ± 0.015	0.112 ± 0.014	0.181 ± 0.009[a]	0.250 ± 0.009[a]
Myo-Inositol	0.077 ± 0.039	0.092 ± 0.024	0.112 ± 0.003[a]	0.181 ± 0.003[a]
NAA	0.063 ± 0.005	0.069 ± 0.003	0.063 ± 0.001[a]	0.093 ± 0.001[a]
Taurine	0.047 ± 0.076	0.080 ± 0.009[a]	0.130 ± 0.024[a]	0.141 ± 0.004[a]
tCholine	0.052 ± 0.004	0.054 ± 0.002	0.059 ± 0.001[a]	0.064 ± 0.002[a]
tCreatine	0.088 ± 0.004	0.087 ± 0.003	0.095 ± 0.001[a]	0.107 ± 0.001[a]

Note: Results are listed for all spectral fitting methods as estimated value ± the corresponding error estimate. Data for $\Delta = 50$ can be found in Supporting Information Table S3 in Appendix S1.

[a]Indicates that the error represents the CRLB estimated in simultaneous fitting, whereas other errors are calculated by the diffusion in python analysis based on the estimated areas from FiTAID.

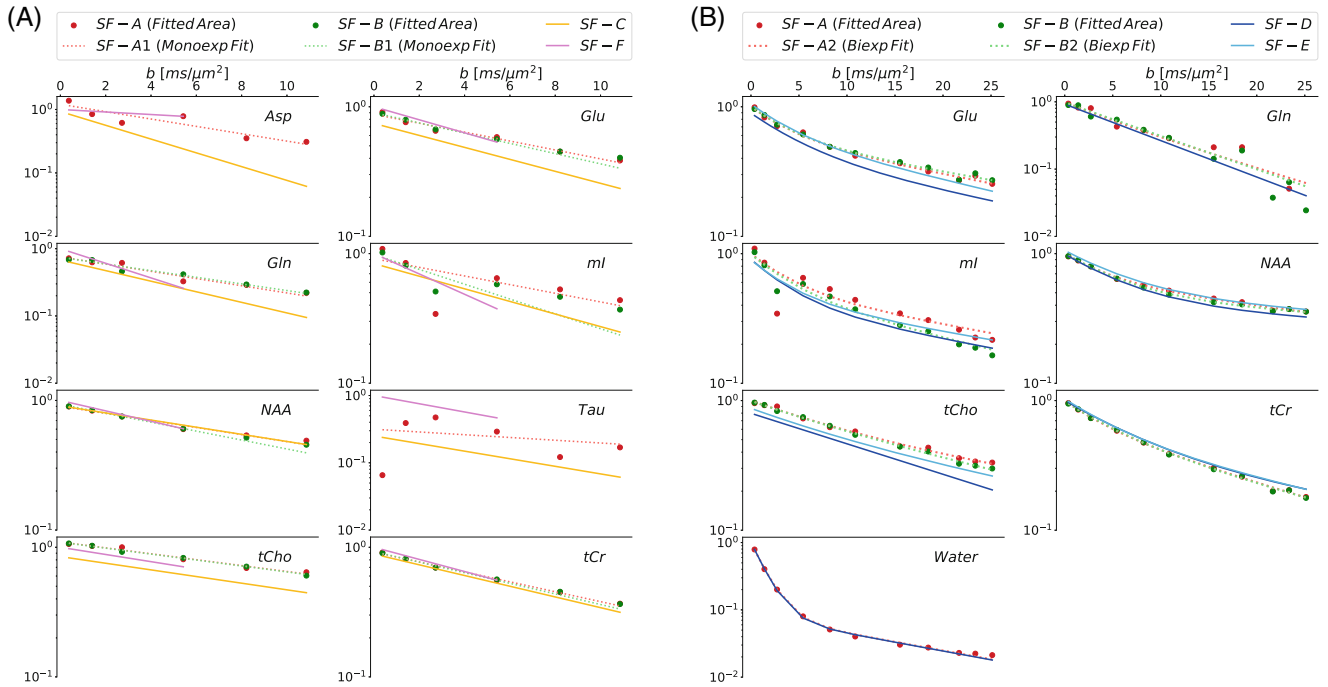

FIGURE 5 Diffusion attenuation estimated for some metabolites as found for the different fitting/modeling schemes for $\Delta = 80$ ms. Monoexponential (A) and biexponential (B) diffusion attenuation of some metabolites obtained from multiple fitting strategies. Dotted lines indicate diffusion signals determined from estimated signal areas (circles) in the subsequent diffusion analysis, whereas in SF-C, SF-D, SF-E, SF-F, the diffusion signal was estimated by simultaneous fitting. Beware that for monoexponential decay estimation in part A, data were restricted to $b < 11$ ms/μm^2 for SF-A1, SF-B1, and SF-C, and to $b < 6$ ms/μm^2 for SF-F. The signal decays are plotted on consistent vertical scales. Differences in estimated amplitudes at b = 0 ms/μm^2 reflect different estimated metabolite contents and possibly differences in the simultaneously determined underlying MMBG signal.

further metabolites are collected in Table S5 in Appendix S1. Estimated metabolite ADCs are fairly consistent throughout the different schemes, although scheme SF-F should be considered as yielding best estimates.

Figure 5B demonstrates the biexponential representation for the expected non-Gaussian diffusion attenuation of the "major" metabolites and water as determined by the different fit strategies. The corresponding numerical

TABLE 3 Estimated model parameters from biexponential fitting of the cohort average spectra with multiple models juxtaposed to data from the literature

Metabolite	Study/species	TE [ms]	Δ [ms]	Case Label	ADC_{fast} [μm²/ms]	ADC_{slow} [μm²/ms]	f_{fast}
Glutamate	Current study	30	80	SF-A3	0.250 ± 0.048	0.033 ± 0.013	0.42 ± 0.16
				SF-B	0.246 ± 0.069	0.029 ± 0.008	0.44 ± 0.09
				SF-D	0.195 ± 0.027[a]	0.034 ± 0.006[a]	0.51
				SF-E	$\mathbf{0.236 \pm 0.027}$[a]	$\mathbf{0.039 \pm 0.004}$[a]	**0.44**
	Rat[10]	22	121.7		0.30 ± 0.02	0.026 ± 0.002	0.5 ± 0.02
Glutamine	Current study	30	80	SF-A3	0.238 ± 0.211	(0.030)	(0.500)
				SF-B	0.114 ± 0.009	—	1.0 ± 0.0
				SF-D	0.125 ± 0.051[a]	—	1
				SF-E	$\mathbf{0.225 \pm 0.027}$[a]	(0.030)	(0.500)
Myo-Inositol	Current study	30	80	SF-A3	0.250 ± 9.192	0.030 ± 0.071	0.48 ± 0.76
				SF-B	0.250 ± 0.003	0.041 ± 0.045	0.48 ± 0.49
				SF-D	0.250 ± 0.014[a]	0.032 ± 0.003[a]	0.55 ± 0
				SF-E	$\mathbf{0.250 \pm 0.017}$[a]	$\mathbf{0.029 \pm 0.002}$[a]	$\mathbf{0.51 \pm 0}$
	Rat[10]	22	121.7		0.24 ± 0.02	0.037 ± 0.003	0.51 ± 0.05
	Mouse[32]	33.4	64.2		0.198 ± 0.034	0.029 ± 0.09	0.51 ± 0.12
NAA	Current study	30	80	SF-A3	0.225 ± 0.006	0.021 ± 0.006	0.39 ± 0.07
				SF-B	0.169 ± 0.030	0.010 ± 0.008	0.56 ± 0.08
				SF-D	0.162 ± 0.006[a]	0.010 ± 0.002[a]	0.59 ± 0
				SF-E	$\mathbf{0.152 \pm 0.006}$[a]	$\mathbf{0.010 \pm 0.002}$[a]	$\mathbf{0.57 \pm 0}$
	Rat[10]	22	121.7		0.27 ± 0.01	0.024 ± 0.001	0.51 ± 0.01
	Mouse[32]	33.4	64.2		0.220 ± 0.023	0.019 ± 0.002	0.49 ± 0.03
tCholine	Current study	30	80	SF-A3	0.100 ± 0.018	0.024 ± 0.062	0.47 ± 1.26
				SF-B	0.100 ± 0.123	0.035 ± 0.047	0.35 ± 1.3
				SF-D	-	0.054 ± 0.005[a]	0
				SF-E	$\mathbf{0.106 \pm 0.046}$[a]	$\mathbf{0.032 \pm 0.013}$[a]	**0.39**
	Rat[10]	22	121.7		0.22 ± 0.03	0.034 ± 0.003	0.49 ± 0.05
	Mouse[32]	33.4	64.2		0.176 ± 0.011	0.024 ± 0.005	0.52 ± 0.06
tCreatine	Current study	30	80	SF-A3	0.250 ± 0.023	0.051 ± 0.005	0.35 ± 0.07
				SF-B	0.195 ± 0.062	0.047 ± 0.011	0.42 ± 0.16
				SF-D	0.140 ± 0.006[a]	0.028 ± 0.003[a]	0.62
				SF-E	$\mathbf{0.177 \pm 0.009}$[a]	$\mathbf{0.038 \pm 0.002}$[a]	**0.5**
	Rat[10]	22	121.7		0.27 ± 0.01	0.027 ± 0.001	0.49 ± 0.02
	Mouse[32]	33.4	64.2		0.191 ± 0.033	0.023 ± 0.005	0.6 ± 0.09
Water	Current study	30	50	SF-A3	0.722 ± 0.038	0.080 ± 0.023	0.92 ± 0.02
				SF-D	$0.803 \pm 2 \times 10^{-5}$[a]	$0.115 \pm 6 \times 10^{-6}$[a]	0.88
			80	SF-A2	0.721 ± 0.017	0.059 ± 0.006	0.92 ± 0.01
				SF-D	$0.741 \pm 1 \times 10^{-5}$[a]	$0.060 \pm 4 \times 10^{-6}$[a]	0.92
	Mouse[32]	33.4	64.2		0.649 ± 0.120	0.069 ± 0.028	0.91 ± 0.03

Note: Results from SF-E are considered to be most relevant from this study and are, thus, printed in bold.

[a] Indicates that the error represents the CRLB estimated in simultaneous fitting, whereas other errors are calculated by the diffusion in python analysis based on the estimated areas from FiTAID.

results are presented in Table 3 in comparison to literature. Similar ADC values emerged from all fitting schemes, with SF-E highlighted because it best fulfills theoretical constraints. The non-Gaussian diffusion characteristic of water is evident above a diffusion-weighting of ~5 ms/μm^2 and apparently well represented by the biexponential model. Non-Gaussian diffusion properties are apparent for most "major" metabolites—visually most convincing for Glu, NAA, and tCr. SF-E yields well-defined biexponential diffusion characteristics for all major metabolites. However, mI shows a very high ADC $_{\text{fast}}$ (at the parameter space limit).

Illustrative results for evaluating single-subject data are presented in Supporting Information Figure S6 in Appendix S1, which demonstrates the variation of results over the cohort and, thus, indicates the robustness of results.

3.2 | MMBG estimation

Some of the estimated MMBG spectral patterns are presented in Figure 6 (others in Supporting Information Figure S7 in Appendix S1) and the resulting parameterization for SF-E in Supporting Information Data S8 in Appendix S1. The patterns are contrasted with respect to impact of mixing (diffusion) times as obtained with identical fitting method in 6A and effect of modeling method at the same mixing time in 6B. For all cases, the patterns are almost identical from 0 to 1.8 ppm irrespective of mixing time, *b*-value range and fit strategy. In A, it is striking that the MMBG patterns show considerably higher signal intensities for the short TM (lower maximum *b*-value and less T_1-related signal loss in TM) throughout the rest of the spectral range. The fitting methods comparison in part B shows that the monoexponential FiTAID fit (SF-C, restricted *b*-value range) yields the MMBG with highest intensity. Comparing SF-A, SF-D and SF-E, all with the full *b*-value range, the differences for the emerging MMBGs are rather minor except that SF-E consistently shows lowest intensity from 2 to 4 ppm. The constrained biexponential representation for the minor metabolites seems to attribute less signal intensity to the MMBG than the other fit models. Part C1 provides an illustrative comparison of our final diffusion-based MMBG (SF-E) with a conventional T_1-relaxation-based MMBG obtained with the same STEAM-sequence in a different group of subjects. It features considerably less intensity >1.8 ppm. Part C2 contains the surplus of MMBG intensity arrived at if the metabolite-nulling based MMBG (presented in C1) is added to the basis set for fit-strategy SF-E.

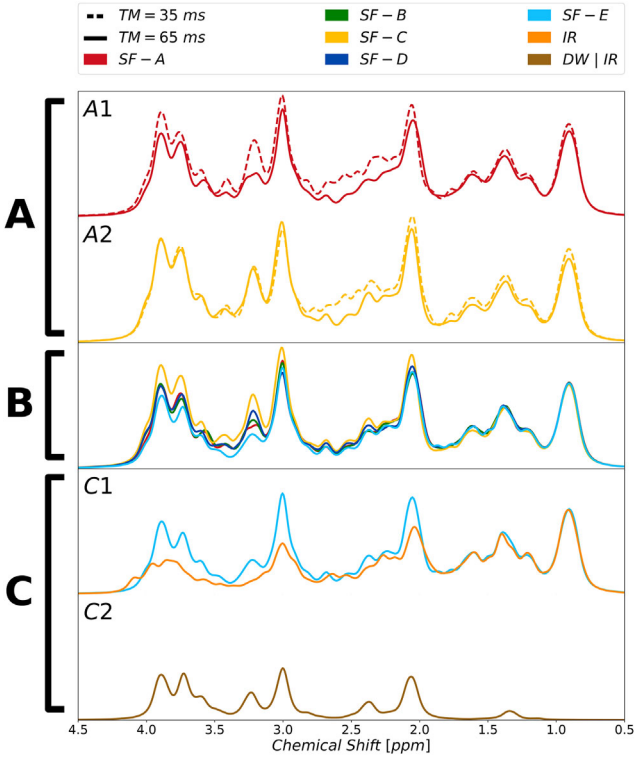

FIGURE 6 Estimated MMBG signal patterns obtained with different fitting strategies at both TM (and diffusion) times (dashed line for TM = 35 ms; solid line for TM = 65 ms). The estimated MMBG patterns are contrasted with respect to different TM times with the same fitting method in (A) and different modeling methods at the same diffusion times in (B). C, The diffusion-based MMBG pattern is contrasted with a MMBG derived from metabolite nulling (IR), i.e., based on relaxation time differences, where in C1 MMBG-IR is overlaid with the presumably best diffusion-based MMBG with enforced biexponential representation (SF-E). Exploring the intensity difference between the two patterns >1.0 ppm, a further 2D fit of the cohort data was performed, where MMBG-IR was included as a base spectrum with mono-exponential signal decay and additional signal from slow-decaying entities was modeled as a second MMBG pattern with the same ADC. This second MMBG pattern (DW|IR) is plotted in C2. It shows broad features at 1.34, 2.075, 2.38, 3.02, 3.25, 3.74, and 3.89 ppm (CH_3 peak of total creatine calibrated as 3.03 ppm). They can represent metabolites in restricted environments with short T_2 (e.g. in mitochondria or intracellular space in myelin sheaths) or macromolecules with longer T_1 or originate from experimental and processing inadequacies. Acquisition and processing details for arriving at MMBG-IR can be found in Supporting Information Text S1 in Appendix S1; MMBG patterns from other strategies are included in Supporting Information Figure S7 in Appendix S1. The parameterization for the pattern of SF-E is provided in Supporting Information Data S8 in Appendix S1.

4 | DISCUSSION

This article reports on in-vivo diffusion characterization of metabolite and MM resonances in human brain obtained by MRS with very high diffusion-weighting at short mixing and echo times. Instead of the conventional approach of relying on differences in T_1 for the definition of MM signals, the strong distinction between ADCs of MMs and metabolites is exploited for estimation of the MM background resonances. Moreover, the diffusion characteristics of metabolite signals are investigated at very high *b*-values at short TE for human gray matter, which has previously only been accessible for rodent brain.

4.1 | Limits for strength of diffusion weighting

The current study was conducted on a MR scanner with Connectom gradients[22] currently offering the strongest gradient strengths for use in human subjects. Comparing the gradient strength of 300 mT/m to that of conventional 3T scanners (≤80 mT/m) translates into up to 14 times higher *b*-values. However, maximum attainable *b*-values are limited by PNS/CS[22] rather than hardware performance under the conditions for human brain MRS. Therefore, a simulation tool[23,24] was used to explore stimulation limits for the allowed parameter range (slew rate and gradient strength on all axes) for STEAM with different echo and mixing times. Phantom measurements were also needed to verify the calculations and probe the parameter space for typical VOI orientations. As a compromise for large *b*-value (short TE and medium TM) 140 mT/m on each axis in the patient coordinate system turned out to be the highest allowed gradient amplitude, yielding $b = 25.1$ ms/μm^2. Stimulation limits, thus, reduced the benefit from the Connectom system to a factor of 3 for the chosen diffusion-weighting scheme.

4.2 | Motion compensation

Cardiac motion-related signal loss was minimized by peripheral triggering during acquisition. Residual motion-related signal loss was mitigated through two compensation schemes in postprocessing. First, a water signal-based method was applied in analogy to that in Ref.[23] However, peripheral triggering with signal modulation from varying effective TRs complicates the definition of motion-related signal loss. T_1-saturation correction of the water signal intensities was, therefore, applied to improve the definition of the motion-free reference level[23,34] needed for amplitude correction for each shot (Figure 1). Given the faster diffusion of water compared to metabolites, the efficiency of W-MoCom decreases substantially with high diffusion-weighting. Hence, a secondary motion-compensation scheme based on MM signals,[31] called M-MoCom, was introduced to eliminate residual motion artifacts. This was applicable to human DW-MRS due to fairly short TE and TM values in our study, while earlier examinations required long TE leading to insufficient MM signal. Still, M-MoCom could only be applied to the averaged spectrum per *b*-value. It remained, therefore, important to use the simultaneously acquired water signal for phase-definition in single acquisitions to guarantee coherent addition of individual acquisitions. To apply signal amplitude corrections in M-MoCom, an undistorted reference diffusion decay of the MM signals had to be estimated first. This was possible using the cohort average from the most reliable individual subject data (ADC <0.010 μm^2/ms, examples in Figure 2) and the isolated 0.9 ppm MM signal. The estimated ADC for MMs of 0.003 μm^2/ms is slightly lower than that found in rodent brain studies (0.006,[10] 0.007,[18] 0.005[32] μm^2/ms)[2] and, thus, seems to represent actual MM diffusion, rather than residual motion-related effects. This also proves the successful combination of the two motion-compensation methods.

Even though M-MoCom can correct for motion-related signal decay at high *b*-values, it should be realized that it may also introduce erroneous signal variation because the low SNR of the $M_{0.94}$ peak in individual spectra entails the risk of imperfect fitting with related miscorrection and amplitude errors of all metabolite signals for this *b*-value. Such a case is seen in Figure 2, where the diffusion signal obtained from subject 3 shows a similar signal decay as for the cohort, but the first point is much lower than expected. This produces a large correction factor at the lowest *b*-value, which is most likely not motion-related but due to an improper model fit. Manual review of suspected misfits with subsequent improved fitting or skipping of the M-MoCom or elimination of this data point can be considered as remedy but is tedious and may introduce bias.

4.3 | Fitting models and methods

With regard to different fitting and signal modeling strategies, maximal robustness for estimated parameters can be introduced when fitting the spectral and diffusion dimensions simultaneously as opposed to fitting spectra independently (i.e., without amplitude-relation) followed by diffusion decay modeling of the estimated signal areas (SF-A). This benefit comes at the cost of being limited to the representations for the diffusion signal decay implemented in

the spectral fit program. With FiTAID, this means that the diffusion-related signal decay has to be exponential, where the monoexponential case had been used before[30] and the biexponential representation was introduced for this study by inserting two independent signals with monoexponential decay, each describing the same metabolite. For *b*-values extending to >20 ms/μm^2 as used here, it seems advisable to allow for biexponential decays for all metabolites[32] except for MM signals. However, such a general approach introduces an excessive number of variables that is prone to overfitting. Non-Gaussian diffusion with estimation of all relevant parameters was, therefore, only implemented for so-called major metabolites with substantial signal representation (according to a heuristic definition). Accordingly, minor metabolites were represented with a Gaussian diffusion model in some of the strategies in spite of the large *b*-value range (SF-B, SF-D) and with somewhat restricted *b*-value range (SF-C,) where a monoexponential decay model may be sufficient considering the limited SNR. The finally developed model SF-E, however, used the full *b*-value range for MMBG definition and biexponential signal representation for all metabolites, but relied on prior knowledge for those decay parameters that do not show large variance in the literature[32] and where SNR is insufficient for their estimation. The biexponential representation for all metabolites is crucial in the determination of the MMBG since MMBG pattern areas (Voigt-line intensities) would compensate for any metabolite signal included in the measured data but not represented in the metabolite model. It is, therefore, not surprising that SF-E yielded the lowest MMBG intensities in areas where the MMBG overlaps with metabolite signals.

4.4 | ADC estimations

ADC estimates obtained with various fitting strategies are reasonably consistent overall but have major disparities in some cases. This is not surprising, given the differences in the employed priors. For Gaussian diffusion (Table 2, Supporting Information Table S3 in Appendix S1), ADC estimates for major metabolites tend to be larger for simultaneous fitting. SF-F with *b*-values restricted to <6 ms/μm^2 yields even higher values than SF-C indicating that the lower estimates are biased by non-Gaussian diffusion >5.5 ms/μm^2[35] The final optimized strategy SF-F, which is based on the MMBG-pattern from SF-E, profits from concentration constraints and is defined on the shortest *b*-value range. It yields values that are in very good agreement with literature for human and animal brain (Figure 7). There are two to three outliers for metabolites at one of the two diffusion times where limited differentiation with other spectral metabolite patterns is the likely cause (Gln vs. Glu, mI vs. Gly). An experimental approach targeted at the monoexponential range smaller *b*-values) would probably render less variability. The ADC values at the shorter diffusion time tend to be higher, in-line with expectation,[36,37] although this study did not really aim at definition of diffusion time dependence of ADCs, the two diffusion times were just a side-product of two alternative settings to define the MMBG. In strategies with simultaneous MMBG determination and in particular for the shorter diffusion time, it appears that multiple ADCs (Glu, Gln, Asp, GSH, EA, PE) were overestimated and the resulting MMBG intensity adjusted at the respective resonance positions to compensate. This indicates that simultaneous definition of MMBG and metabolite ADCs can lead to ambiguous results when using a limited *b*-value range. Therefore, predefining the MMBG pattern with higher *b*-values and using a limited *b*-value range to estimate metabolite ADCs in a second step, as done in SF-F, is advantageous.

In non-Gaussian diffusion analysis, it can be disputed for which settings a biexponential model is sufficient to represent[38] metabolite diffusion data. Figure 5B confirms that this choice adequately describes the experimental data for the *b*-value range achieved in this study. Only the water data may suggest a slight deviation from the model at very high *b*-values. Ligneul et al.[32] have used this model for metabolite diffusion previously, even closely fitting the experimental data at higher *b*-values. The difficulties with describing non-Gaussianity in our study relates more to the fact that a reliable definition of biexponential decays bases on sufficient coverage of the relevant *b*-value range and can only succeed if the ADCs of the two components are sufficiently distinct. Some of the results in Table 3 clearly raise doubts in this respect for almost all metabolites. Only for NAA and Glu, the fast component fraction is defined with less than 20% error in SF-B where diffusion modeling is performed as a separate step. In concurrent spectral and diffusion signal modeling (SF-D, SF-E) this error is not available since FiTAID provides CRLB for the fit parameters only, and the fractions are calculated from the component amplitudes.[3] However, considering CRLB of component sizes and ADCs, it appears that simultaneous fitting is, in principle, able to define these parameters with remarkable precision: The areas of almost all metabolites are defined with relative CRLB <∼10%. This also applies to the ADCs with CRLB <20% for almost all metabolites in both components. Of note, this assessment is inherently overoptimistic being based on the assumption that the fit model is correct, and that variance is equal between and within

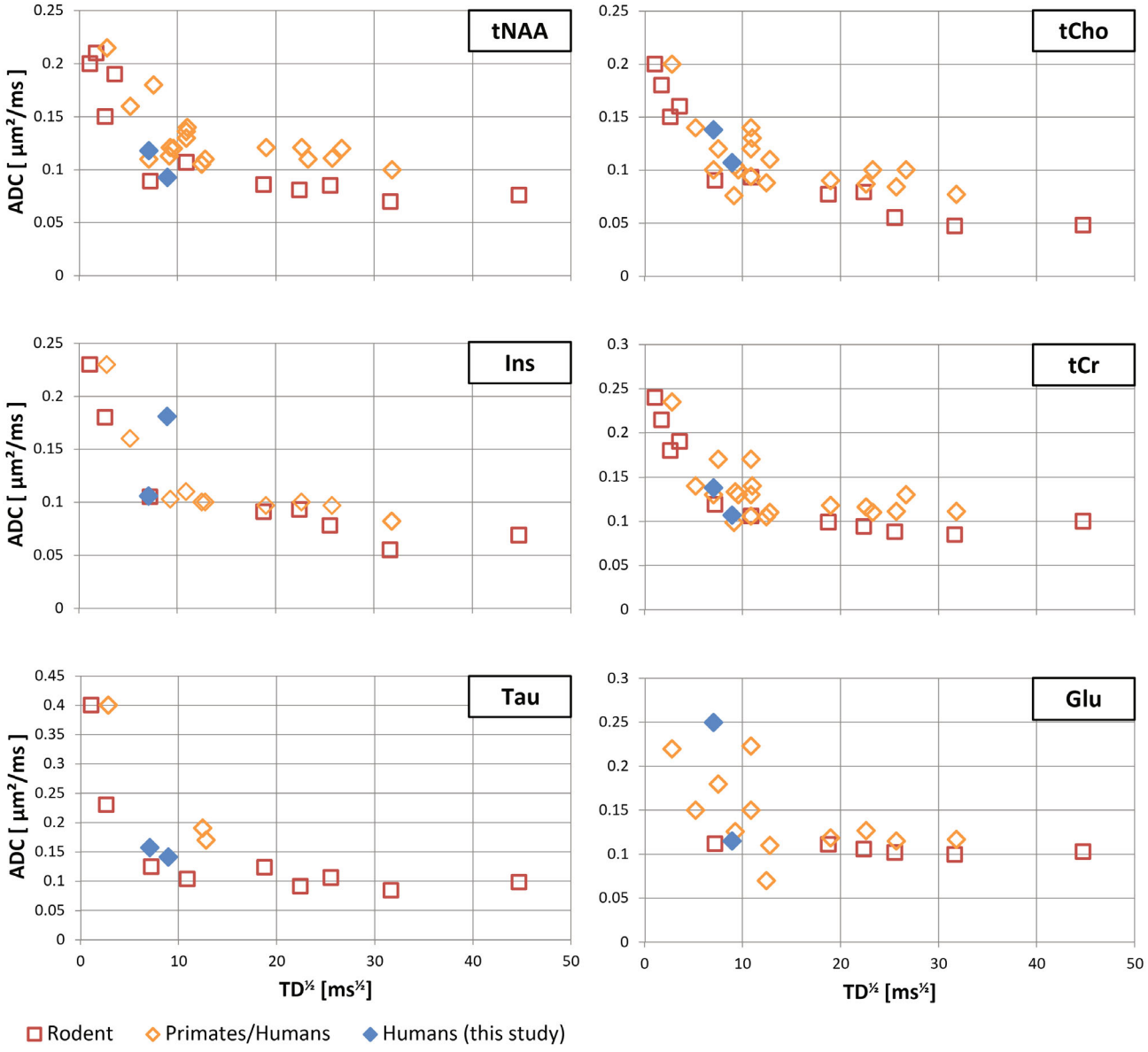

FIGURE 7 Illustration of estimated monoexponential metabolite diffusion constants found in this study in comparison to literature results[10,23,31,37,41–49] for animals and humans. The plots provide values as function of diffusion time to ease the comparison even though the current study was not targeting this dependence. The ADC values estimated with strategy SF-F are plotted for this study.

spectra, i.e., due to random noise without contributions from variations between sequentially obtained spectra. Hence, it only defines a lower bound of the real error. Nevertheless, this analysis suggests that the simultaneous fit model is well suited for the definition of biexponential diffusion decays in the current setup. Given that the errors in subsequent modeling are similar to the CRLB in simultaneous modeling for some of the major metabolite ADCs, it appears that the CRLB provide reasonable estimates of real errors. In summary, this suggests that all bi-exponentially represented metabolites indeed show non-Gaussian decays in their data, maybe with the exception of mI, where ADC_{fast} is likely overestimated due to artifacts around 3.4 ppm in the lowest diffusion-weighted spectra, and tCho, where the ADCs are only a factor 3 apart in SF-E and no second component was found in SF-D.

SF-E is expected to provide the most accurate results, given the biexponential decay for all metabolites and the restriction of metabolite contents to meaningful values (see Supporting Information Text S1 in Appendix S1). The enforced parameters for minor metabolites are well in-line with the estimated values for the major metabolites, and potential deviations of true values from those in the prior are not expected to have substantial influence given the SNR in the data.

There are few data in the literature with which to compare, first because the current study is unique for humans and second because animal studies often did not include a biexponential representation. Still, mouse[32] and rat data[10] (Table 3) are in-line with the current results (especially for SF-E), despite different acquisition methods (incl. *b*-value range) and species. As in the literature, the relative fractions of both components are near 50% for all metabolites (and f_{fast} at 90% for water). One clear deviation from literature is seen for NAA where the current study yields a smaller ADC for both components-in particular ADC_{slow} is even limited by the lower boundary. A preliminary analysis using a MMBG from metabolite-nulling instead of the diffusion-based MMBG confirms the main results, although the slow ADC tends to even smaller values and thus the non-Gaussian characteristic would appear even stronger.

4.5 | MMBG determination

The definition of the MMBG signal pattern usually exploits T_1-differences for MM vs. metabolite signals, which entails challenges to properly compensate for differences in T_1 between different metabolite signals and modest T_1 differences between MMs and some metabolites. Here, we base this definition on the large difference in molecular size reflected in >30 times slower diffusion of MMs compared to small metabolites. For most accurate and undistorted determination of MMBG signals, it is crucial to use a short TE to prevent T_2-related signal loss. Additionally, a short TM mitigates alterations of the MM pattern due to differing T_1 values of its constituents. It is nevertheless essential to apply very strong *b*-values to achieve a sufficient suppression of metabolite signals. Fulfilling these conditions is achieved with a Connectom gradient system. Still, since complete suppression of metabolite signals is impossible—due to constraints imposed by stimulation limits, but also considering non-Gaussian metabolite diffusion due to brain microstructure—the acquisition scheme has to be combined with appropriate diffusion signal modeling, ideally in a simultaneous spectral/diffusion fitting scheme. Earlier preliminary results from a standard clinical scanner were based on somewhat longer TE, substantially longer TM, and rather modest diffusion-weighting (5.2 ms/μm^2).[39]

For the different fitting approaches used here, only minor differences appeared in the final MMBG patterns. The definition is clearly more consistent when extending the *b*-value range to >20 ms/μm and considering biexponential decay. Some of the differences between shorter and longer diffusion times could be attributable to T_1 signal decay of MMBG resonances during TM (Figure 6A). The MMBG pattern differences between fitting approaches ms are likely due to the limited precision in the definition of the metabolite ADCs for some of the minor metabolites, particularly with subsequent diffusion modeling without amplitude bounds when fitting the high *b*-value spectra. Given the consistent results for metabolite diffusion confirming the imposed priors, SF-E is expected to provide the most accurate estimate for the MMBG pattern, where the non-Gaussian diffusion component is taken into account also for the minor metabolites.

Even when applying optimized methodology, a DW-based definition of the MMBG pattern is still restricted by inherent limits of the approach. One is the unknown composition of the MMBG, which was tackled by using a versatile general signal representation with equally spaced Voigt lines, which is flexible to adapt to the actual pattern but may be prone to overfitting. The main basic limit, however, is due to the complex diffusion decay of metabolite signals. The non-Gaussian diffusion is hard to accurately represent in the limited *b*-value regime and with the limited SNR. Additionally, any signals from metabolites that are restricted to small compartments within the diffusion time would be indistinguishable from MM signals. When comparing the diffusion- with relaxation-based MMBG (Figure 6C), appreciable differences are observed. While the characteristics are similar <1.8 ppm, the MMBG pattern from the diffusion-based definition shows more intensity, in particular near or/at resonance positions of prominent metabolite features (2.0, 3.0, 3.2, 3.7–3.9 ppm). A preliminary combined analysis with a metabolite-nulling MMBG and a diffusion-based extension confirms the visual difference. These differences can be due to spatially restricted and T_2-broadened metabolites in general (possibly echoing a reported transverse relaxation time dependence of the ADC of creatines in human brain[40] although not confirmed in rodents[32]) or the enforced prior of equal ADCs for Cr and PCr; but part of this discrepancy can also be due to macromolecular signals with longer T_1s (side chain mobility, partial signal suppression by the inversion recovery method) or experimental inaccuracies, e.g., stemming from removal of metabolite signals (often done in a heuristic fashion).

4.6 | Limitations

4.6.1 | Data

The data at the lowest *b*-values (0.37 and 1.4 ms/μm^2) showed artifacts around 3.5 and 3.9 ppm for some subjects, probably due to spurious echoes. Even though evidently corrupted data were not used, it is unclear whether the fast ADC found for Glc is real (and corroborating expectation

for a partially interstitial metabolite) or due to remaining artifacts. This could also affect the mI resonance.

4.6.2 | Model

The MMBG model is heuristic, and the parameterization could have a certain influence. The restrictions enforced in the diffusion model are also partly arbitrary, in particular the differentiation into minor and major metabolites. Other choices taken for the diffusion and spectral models, although well rationalized, could also be disputed, such as the assumption of identical diffusion behavior for composite peaks despite their different molecular size and potentially different cellular distribution (PCho/GPC; Cr/PCr). Moreover, Cr and PCr were modeled with equal concentrations to limit the overall fit flexibility because initial trials with fewer constraints yielded implausible results. Amplitude restraints to keep concentrations within a physiologically reasonable range (which was somewhat questionable for the smaller *b*-value range) were only introduced for SF-A3, SF-E, and SF-F. Estimated metabolite ADC values from mouse data[32] were used as prior in defining the upper boundary (0.25 μm^2/ms) in the simultaneous fit, while the lower bound (0.01 μm^2/ms) was imposed to guarantee a clear differentiation to the MMs. Still, some metabolite ADCs ended up at the upper or lower bounds.

5 | CONCLUSIONS

DW-MRS at high diffusion-weighting offers an alternative for definition of the MMBG signal pattern that is essential to be known for robust fitting of clinical ^{1}H-MR spectra. Covering a *b*-value range up to 25.1 ms/μm^2 and simultaneous spectral/diffusion fitting allowed for appropriate modeling of the spectral signals under the constraints of the diffusion signal decay. This turned out to be beneficial for both, the definition of the MMBG pattern, but also the determination of metabolite diffusion characteristics. Biexponential signal representation was both essential and sufficient for the major metabolite signals and also the concurrently acquired water signal. Motion-compensation using the water signal and a macromolecular signal prevented artifactual signal decay that would bias the diffusion evaluation. Even higher diffusion-weighting would be beneficial but was limited by physiologic stimulation in the current study. Intrinsic limitations to distinguish non-Gaussian metabolite signal decay or contributions of physically restrained metabolites from macromolecular signals must be taken into account and may contribute to differences with respect to relaxation-based macromolecular spectra.

ACKNOWLEDGMENT

This work is supported by the Swiss National Science Foundation (SNSF #320030-175984, 202962).

ENDNOTES

[1] *Following the convention introduced in the consensus paper of Ref*[4] *this peak is labeled* $M_{0.94}$*, even though at 3 T it is centered rather at 0.92 ppm.*

[2] *Ref* 32 found different values depending on the b-value range (and indications for biexponential behavior) and also a trend for a TE-dependence. In the current study, the estimated ADC for MMs was 0,008 µm2/ms if no individual data with faster decay was excluded.

[3] Straight-forward error propagation cannot be applied to determine a CRLB of the component fraction since the CRLBs are correlated.

ORCID

André Döring https://orcid.org/0000-0002-2096-5374
Harald E. Möller https://orcid.org/0000-0002-5659-1925
Roland Kreis https://orcid.org/0000-0002-8618-6875

REFERENCES

1. Öz G, Alger JR, Barker PB, et al. Clinical proton MR spectroscopy in central nervous system disorders. *Radiology*. 2014;270:658-679.
2. Behar KL, Ogino T. Characterization of macromolecule resonances in the 1H NMR spectrum of rat brain. *Magn Reson Med*. 1993;30:38-44.
3. Behar KL, Rothman DL, Spencer DD, Petroff OAC. Analysis of macromolecule resonances in 1H NMR spectra of human brain. *Magn Reson Med*. 1994;32:294-302.
4. Cudalbu C, Behar KL, Bhattacharyya PK, et al. Contribution of macromolecules to brain 1H MR spectra: Experts' consensus recommendations. *NMR Biomed*. 2021;34:e4393. doi:10.1002/nbm.4393
5. Cudalbu C, Mlynárik V, Gruetter R. Handling macromolecule signals in the quantification of the neurochemical profile. *J Alzheimers Dis*. 2012;31:S101-S115.
6. Near J, Harris AD, Juchem C, et al. Preprocessing, analysis and quantification in single-voxel magnetic resonance spectroscopy: experts' consensus recommendations. *NMR Biomed*. 2021;34:e4257. doi:10.1002/nbm.4257
7. Seeger U, Klose U, Mader I, Grodd W, Nägele T. Parameterized evaluation of macromolecules and lipids in proton MR spectroscopy of brain diseases. *Magn Reson Med*. 2003;49:19-28.
8. Mlynrik V, Gruber S, Moser E. Proton T1 and T2 relaxation times of human brain metabolites at 3 tesla. *NMR Biomed*. 2001;14:325-331.
9. Xin L, Schaller B, Mlynarik V, Lu H, Gruetter R. Proton T1 relaxation times of metabolites in human occipital white and gray matter at 7 T. *Magn Reson Med*. 2013;69:931-936.
10. Pfeuffer J, Tkáč I, Gruetter R. Extracellular-intracellular distribution of glucose and lactate in the rat brain assessed noninvasively by diffusion-weighted 1H nuclear magnetic resonance spectroscopy in vivo. *J Cereb Blood Flow Metab*. 2000;20:736-746.

11. Cudalbu C, Mlynrik V, Xin L, Gruetter R. Quantification of in vivo short echo-time proton magnetic resonance spectra at 14.1 T using two different approaches of modelling the macromolecule spectrum. *Meas Sci Technol.* 2009;20:104034. doi:10.1088/0957‐0233/20/10/104034
12. Cudalbu C, Beuf O, Cavassila S. In vivo short echo time localized 1H MRS of the rat brain at 7 T: influence of two strategies of background-accommodation on the metabolite concentration estimation using QUEST. *J Signal Process Syst*. 2009;55:25-34.
13. Provencher SW. Estimation of metabolite concentrations from localized in vivo proton NMR spectra. *Magn Reson Med*. 1993;30:672-679.
14. Giapitzakis IA, Avdievich N, Henning A. Characterization of macromolecular baseline of human brain using metabolite cycled semi-LASER at 9.4T. *Magn Reson Med*. 2018;80:462-473.
15. Hofmann L, Slotboom J, Boesch C, Kreis R. Characterization of the macromolecule baseline in localized 1H-MR spectra of human brain. *Magn Reson Med*. 2001;46:855-863.
16. Chong DGQ, Kreis R, Bolliger CS, Boesch C, Slotboom J. Two-dimensional linear-combination model fitting of magnetic resonance spectra to define the macromolecule baseline using FiTAID, a fitting tool for arrays of interrelated datasets. *Magn Reson Mater Phys Biol Med*. 2011;24:147-164.
17. Hoefemann M, Bolliger CS, Chong DGQ, van der Veen JW, Kreis R. Parameterization of metabolite and macromolecule contributions in interrelated MR spectra of human brain using multidimensional modeling. *NMR Biomed*. 2020;33:e4328. doi:10.1002/nbm.4328
18. Kunz N, Cudalbu C, Mlynarik V, Hüppi PS, Sizonenko SV, Gruetter R. Diffusion-weighted spectroscopy: a novel approach to determine macromolecule resonances in short-echo time 1H-MRS. *Magn Reson Med*. 2010;64:939-946.
19. Ronen I. Valette J diffusion-weighted magnetic resonance spectroscopy. *eMagRes*. 2015;4:733-750.
20. Cao P, Wu EX. In vivo diffusion MRS investigation of non-water molecules in biological tissues. *NMR Biomed*. 2017;30:e3481. doi:10.1002/nbm.3481
21. Palombo M, Shemesh N, Ronen I, Valette J. Insights into brain microstructure from in vivo DW-MRS. *Neuroimage*. 2018;182:97-116.
22. Setsompop K, Kimmlingen R, Eberlein E, et al. Pushing the limits of in vivo diffusion MRI for the human connectome project. *Neuroimage*. 2013;80:220-233.
23. Döring A, Adalid V, Boesch C, Kreis R. Diffusion-weighted magnetic resonance spectroscopy boosted by simultaneously acquired water reference signals. *Magn Reson Med*. 2018;80:2326-2338.
24. Şimşek K, Döring A, Pampel A, Möller HE, Kreis R. Diffusion-weighted MRS at short TE using a Connectom system: non-Gaussian metabolite diffusion and macromolecular signals in human brain. In: *Proceedings of the Virtual Conference of ISMRM*; 2020:0364.
25. Hebrank FX, Gebhardt M. SAFE-model -- a new method for predicting peripheral nerve stimulations in MRI. In: *Proceedings of the 8th Annual Meeting of ISMRM, Denver, CO, USA*; 2000:2007.
26. Szczepankiewicz F, Westin CF, Nilsson M. Maxwell-compensated design of asymmetric gradient waveforms for tensor-valued diffusion encoding. *Magn Reson Med*. 2019;82:1424-1437.
27. Simpson R, Devenyi GA, Jezzard P, Hennessy TJ, Near J. Advanced processing and simulation of MRS data using the FID appliance (FID-A)—an open source, MATLAB-Based Toolkit. *Magn Reson Med*. 2017;77:23-33.
28. Hall EL, Stephenson MC, Price D, Morris PG. Methodology for improved detection of low concentration metabolites in MRS: optimised combination of signals from multi-element coil arrays. *Neuroimage*. 2014;86:35-42.
29. Stefan D, Di CF, Andrasescu A, et al. Quantitation of magnetic resonance spectroscopy signals: the jMRUI software package. *Meas Sci Technol*. 2009;20:104035. doi:10.1088/0957‐0233/20/10/104035
30. Adalid V, Döring A, Kyathanahally SP, Bolliger CS, Boesch C, Kreis R. Fitting interrelated datasets: metabolite diffusion and general lineshapes. *Magn Reson Mater Phys Biol Med*. 2017;30:429-448.
31. Ligneul C, Valette J. Probing metabolite diffusion at ultra-short time scales in the mouse brain using optimized oscillating gradients and "short"-echo-time diffusion-weighted MRS. *NMR Biomed*. 2017;30:e3671. doi:10.1002/nbm.3671
32. Ligneul C, Palombo M, Valette J. Metabolite diffusion up to very high b in the mouse brain in vivo: revisiting the potential correlation between relaxation and diffusion properties. *Magn Reson Med*. 2017;77:1390-1398.
33. Palombo M, Ligneul C, Valette J. Modeling diffusion of intracellular metabolites in the mouse brain up to very high diffusion-weighting: diffusion in long fibers (almost) accounts for non-monoexponential attenuation. *Magn Reson Med*. 2017;77:343-350.
34. Şimşek K, Döring A, Pampel A, Möller HE, Kreis R. Simultaneous spectral and bi-exponential diffusion modeling of doubly motion-corrected human brain spectra with very high b-values. In: *Proceedings of the Annual Meeting of ISMRM*; 2021:4263.
35. Genovese G, Marjańska M, Auerbach EJ, et al. In vivo diffusion-weighted MRS using semi-LASER in the human brain at 3 T: methodological aspects and clinical feasibility. *NMR Biomed*. 2021;34:e4206. doi:10.1002/nbm.4206
36. Valette J, Ligneul C, Marchadour C, Najac C, Palombo M. Brain metabolite diffusion from ultra-short to ultra-long time scales: what do we learn, where should we go? *Front Neurosci*. 2018;12:2.
37. Döring A, Kreis R. Magnetic resonance spectroscopy extended by oscillating diffusion gradients: cell-specific anomalous diffusion as a probe for tissue microstructure in human brain. *Neuroimage*. 2019;202:116075. doi:10.1016/j.neuroimage.2019.116075
38. Novikov DS, Kiselev VG, Jespersen SN. On modeling. *Magn Reson Med*. 2018;79:3172-3193.
39. Döring A, Adalid V, Boesch C, Kreis R. On the exploitation of slow macromolecular diffusion for baseline estimation in MR spectroscopy using 2D simultaneous fitting. In: *Proceedings of the 26th Annual Meeting of ISMRM, Paris, France*. 2018:1315.
40. Branzoli F, Ercan E, Webb A, Ronen I. The interaction between apparent diffusion coefficients and transverse relaxation rates of human brain metabolites and water studied by diffusion-weighted spectroscopy at 7 T. *NMR Biomed*. 2014;27:495-506.
41. Palombo M, Ligneul C, Najac C, et al. New paradigm to assess brain cell morphology by diffusion-weighted MR spectroscopy in vivo. *Proc Natl Acad Sci USA*. 2016;113:6671-6676.

42. Ellegood J, Hanstock CC, Beaulieu C. Trace apparent diffusion coefficients of metabolites in human brain using diffusion weighted magnetic resonance spectroscopy. *Magn Reson Med*. 2005;53:1025-1032.
43. Valette J, Guillermier M, Besret L, Hantraye P, Bloch G, Lebon V. Isoflurane strongly affects the diffusion of intracellular metabolites, as shown by 1H nuclear magnetic resonance spectroscopy of the monkey brain. *J Cereb Blood Flow Metab*. 2007;27:588-596.
44. Kan HE, Techawiboonwong A, Van Osch MJP, et al. Differences in apparent diffusion coefficients of brain metabolites between grey and white matter in the human brain measured at 7 T. *Magn Reson Med*. 2012;67:1203-1209.
45. Marchadour C, Brouillet E, Hantraye P, Lebon V, Valette J. Anomalous diffusion of brain metabolites evidenced by diffusion-weighted magnetic resonance spectroscopy in vivo. *J Cereb Blood Flow Metab*. 2012;32:2153-2160.
46. Najac C, Marchadour C, Guillermier M, et al. Intracellular metabolites in the primate brain are primarily localized in long fibers rather than in cell bodies, as shown by diffusion-weighted magnetic resonance spectroscopy. *Neuroimage*. 2014;90:374-380.
47. Ercan AE, Techawiboonwong A, Versluis MJ, Webb AG, Ronen I. Diffusion-weighted chemical shift imaging of human brain metabolites at 7T. *Magn Reson Med*. 2015;73:2053-2061.
48. Deelchand DK, Auerbach EJ, Marjańska M. Apparent diffusion coefficients of the five major metabolites measured in the human brain in vivo at 3T. *Magn Reson Med*. 2018;79:2896-2901.
49. Ingo C, Brink W, Ercan E, Webb AG, Ronen I. Studying neurons and glia non-invasively via anomalous subdiffusion of intracellular metabolites. *Brain Struct Funct*. 2018;223:3841-3854.

SUPPORTING INFORMATION

Additional supporting information may be found in the online version of the article at the publisher's website.

Appendix S1. Supporting Information.

How to cite this article: Şimşek K, Döring A, Pampel A, Möller HE, Kreis R. Macromolecular background signal and non-Gaussian metabolite diffusion determined in human brain using ultra-high diffusion weighting. *Magn Reson Med*. 2022;1-16. doi: 10.1002/mrm.29367